Article

J. Biol. Regul. Homeost. Agents. 2024; 38(6): 5293–5304
https://doi.org/10.23812/j.biol.regul.homeost.agents.20243806.423

Genome-Wide Profiling of Extracellular Vesicles Derived from B16 Melanoma Cells Reflects Dynamic Changes in Mutation Profiles of Melanoma Cells

Xiulin Chang[1,2], Yanqiu Hua[1,2], Lanxi Wang[1,2], Yongzhu Jiang[1,2], Liaoqiong Fang[1,3], Jin Bai[1,2,*]

[1]State Key Laboratory of Ultrasound in Medicine and Engineering, College of Biomedical Engineering, Chongqing Medical University, 400016 Chongqing, China
[2]Chongqing Key Laboratory of Biomedical Engineering, Chongqing Medical University, 400016 Chongqing, China
[3]National Engineering Research Center of Ultrasound Medicine, 401121 Chongqing, China
*Correspondence: sajinbai@cqmu.edu.cn (Jin Bai)
Submitted: 20 March 2024 Revised: 16 April 2024 Accepted: 7 May 2024 Published: 1 June 2024

Background: Extracellular vesicles (EVs) are carriers of DNA derived from parental cells, presenting a promising avenue for monitoring tumor progression. This aimed to investigate the relationship between EV DNA and the parental cell genome to establish a theoretical foundation for utilizing EVs to dynamically monitor tumor progression.
Methods: Utilizing a classical model of cell tumor evolution, B16 melanoma cell lines (B16-F0, B16-F1, and B16-F10) with varying metastatic potentials, we demonstrated that EVs derived from these cells harbor stable double-stranded (dsDNA) fragments ranging from 15 to 10,000 bp. DNase I enzyme digestion, SYBR Green I staining, and TapeStation system were employed for characterization. Whole genome profiling analysis revealed a high concordance between EV DNA and the mutant spectrum of parent cells, particularly regarding single nucleotide polymorphisms (SNPs). EVs contained evolutionary relevant mutation profile of melanoma cells with different metastatic potentials and had a comparable evolutionary relationship with the parent cells.
Results: (1) EVs derived from B16 melanoma cells contained stable dsDNA fragments ranging from 15 to 10,000 bp. (2) EVs DNA comprehensively covered the entire genome of parent cells. (3) EVs DNA exhibited strong consistency with small fragment mutations (SNPs, Inserts/Deletions) of parent cells, with decreasing consistency as mutation length increased. (4) EVs carried mutant gene profiles associated with melanoma cell progression and had similar evolutionary relationships with parent cells.
Conclusions: This study underscores the ability of EVs DNA to reflect the mutation status of parental cells and emphasizes their potential as biomarkers for monitoring tumor evolution. These findings offer a theoretical foundation for the dynamic monitoring of tumor progression using EVs DNA.

Keywords: melanoma; extracellular vesicles; DNA; mutation; evolution

Introduction

Extracellular vesicles (EVs), small lipid-bilayer membrane vesicles released from nearly all types of cells, are induced by various external stimuli or occur spontaneously [1,2]. Currently, EVs are classified into exosomes, microvesicles, and apoptotic bodies based on their biogenesis, size, and morphology [3–5]. Initially disregarded as mere "cell dust", EVs are now recognized as containing lipids [6–8], RNA [9–11], and proteins [12–14] derived from parent cells, reflecting the physiological and pathological status of parental cells [15–17], thus regarded as potential biomarkers [18].

The revelation that EVs encapsulate DNA has significantly advanced the field [19,20]. Recent studies suggest that EVs DNA mirrors the genomic content of parental cells, shedding light on its potential role in facilitating horizontal gene transfer between cells. This mechanism contributes to genetic diversity and may aid in the dissemination of oncogenic elements during cancer progression [21–23]. Additionally, EVs DNA has been shown to harbor specific genetic alterations present in the original cells, such as mutations or amplifications, suggesting the potential of EVs in non-invasive cancer diagnostics. These observations offer a novel approach for monitoring tumor progression and identifying therapeutic targets through the analysis of tumor-derived DNA in bodily fluids [24–28].

Despite these promising advancements, the application of EVs DNA for dynamically monitoring tumor progression remains in its infancy [29]. Limited comparative studies on the mutational and molecular characteristics of tumors and EVs exist due to the challenge of obtain-

Journal of
BIOLOGICAL REGULATORS
and Homeostatic Agents

ing simultaneous and/or continuous samples of primary and metastatic tumors and their corresponding EVs. The B16 melanoma cell line, derived from C57BL/6 mouse spontaneous melanoma, is a classical tumor cell model. Utilizing B16-F0 as the parent cell line, B16-F1, and B16-F10 cell lines were obtained through repeated *in vivo* selection, all sharing the same genetic background but differing in metastatic potential [30,31]. Study has demonstrated that the metastatic capabilities of the B16 cell line intensify progressively according to the order of F0, F1 and F10, and that the metastatic characteristics remain stable even after multiple *in vitro* cultures [32]. Given that metastatic potential is a crucial indicator of tumor evolution, the B16 melanoma cell lines are regarded as a classical model reflecting tumor evolution. In this study, melanoma cell lines with varying metastatic capabilities (B16-F0, B16-F1, and B16-F10) were examined, with melanocytes (Melan-a) as the physiological control, to elucidate the comprehensive genomic landscape encapsulated within EVs secreted by these cells. The objective was to isolate and characterize all subtypes of EVs originating from the parental cells to assess the fidelity of the mutation spectrum between melanoma-derived EVs and their parental cells. Moreover, this study aimed to determine whether EVs, derived from melanoma cells with distinct metastatic propensities, can accurately mirror the evolutionarily pertinent molecular attributes of the parental cell lineage.

Materials and Methods

Cell Culture

Mouse melanoma cell lines (B16-F0 and B16-F1) were procured from the American Type Culture Collection (ATCC; catalog numbers: CRL-6322, CRL-6323, Manassas, VA, USA). Both cell lines were confirmed to be mycoplasma free and STR analysis confirmed their respective identities. The mouse melanocytes (Melan-a) and mouse melanoma cell line (B16-F10) were obtained from the State Key Laboratory of Ultrasound in Medicine and Engineering (Chongqing, China). Both cell lines underwent rigorous in-house mycoplasma testing and species identification to ensure purity and accuracy. Melan-a and B16-F10 cells were cultured in RPMI-1640 medium (catalog number: 11875119, Gibco, Waltham, MA, USA), while B16-F0 and B16-F1 cells were cultured in DMEM medium (catalog number: C11995500BT, Gibco, Waltham, MA, USA). All media were supplemented with 10% fetal bovine serum (FBS; catalog number: 10099-141, Gibco, Waltham, MA, USA). To minimize potential exosome contamination from FBS, the serum underwent ultracentrifugation at 100,000 $\times$g overnight at 4 °C, followed by filtration through a 0.22 µm filter before being added to the media. Cells were maintained at 37 °C in a 5% CO_2 humidified environment. Passaging was performed bi-daily upon reaching 80%–90% confluence.

EVs Isolation and Purification

Cell-conditioned media (660 mL) from Melan-a, B16-F0, B16-F1, and B16-F10 cells grown to 80%–90% confluence in T175 cell culture flasks were utilized for EVs isolation. EVs were isolated and purified through a combination of differential centrifugation and density gradient centrifugation (Fig. 1A). Initially, EVs were enriched using the previously described method of differential centrifugation [33]. Firstly, samples were centrifuged at 400 $\times$g for 5 minutes to eliminate dead cells and subsequently ultrafiltered through a 1.2 µm Minisart Syringe Filter (catalog number: 17593, Sartorius, Göttingen, Germany). Next, cell debris was removed by centrifugation at 2000 $\times$g for 30 minutes. The resulting supernatant was centrifuged at 10,000 $\times$g for 30 minutes to collect the first EV pellet, EV1. Subsequently, the supernatant was centrifuged at 50,000 $\times$g for 90 minutes to obtain the second EV pellet, EV2. Finally, the remaining supernatant was centrifuged at 100,000 $\times$g for 90 minutes to obtain the third EV pellet, EV3.

Subsequently, the three EV pellets were purified using OptiPrep^{TM} iodixanol density gradients (catalog number: D1556, Sigma-Aldrich, St. Louis, MO, USA) respectively. Iodixanol density gradient buffers of 10%, 35%, and 45% were prepared with PBS. 5 mL layers of 45%, 35%, and 10% iodixanol density gradient buffer were overlaid to form a discontinuous gradient, visually discernible by stratification. The EV pellet was resuspended in 2 mL PBS and added above the discontinuous gradient. EV1 was ultracentrifuged at 10,000 $\times$g for 1 hour, EV2 at 50,000 $\times$g for 3 hours, and EV3 at 100,000 $\times$g for 3 hours. White layers were observed in the interphase of 45%–35% in all samples. These white layers were transferred to new tubes, diluted and washed in 30 mL PBS, and ultracentrifuged (EV1: 10,000 $\times$g for 30 minutes; EV2: 50,000 $\times$g for 90 minutes; EV3: 100,000 $\times$g for 90 minutes). All centrifugations were performed at 4 °C. The EV1, EV2, and EV3 pellets were then collectively resuspended in PBS in a single tube, designated EVs. EVs were either processed immediately or stored at –80 °C.

Nanoparticle Tracking Analysis (NTA)

Nanoparticle tracking analysis was performed as described in a previous study [33]. Briefly, purified EVs (1 µL) were diluted in 1 mL of PBS and quantified using nanoparticle tracking analysis (Nano-sight NS 300, Malvern analytical Ltd., Malvern, UK) to determine size distribution and particle concentration.

Western Blotting Analysis

Western blot analysis followed procedures outlined in a recent publication [33]. EVs were lysed using RIPA lysate (catalog number: P0013B, Beyotime Biotechnology, Shanghai, China) containing PMSF (catalog number: ST506, Beyotime Biotechnology, Shanghai, China). Proteins were separated by SDS-PAGE (catalog number:

P0015, Beyotime Biotechnology, Shanghai, China) using a 12% separation gel and then transferred to a 0.22 μm PVDF membrane (catalog number: ISEQ00010, Millipore, Bedford, MA, USA). The membrane was blocked with 5% non-fat milk in TBST (Solarbio, Beijing, China; catalog number: T1081) for 1 hour. After washing three times with TBST, the membrane was incubated with primary antibodies at 4 °C overnight. The primary antibodies used included Cluster of Differentiation 63 (CD63; 1:1000 dilution; Abcam, Cambridge, UK; catalog number: ab217345), Tumor Susceptibility Gene 101 (TSG101; 1:5000 dilution; Abcam, Cambridge, UK; catalog number: ab125011). The membrane was washed thrice with TBST before incubating with a secondary antibody for 1 hour at 37 °C. The secondary antibody was anti-rabbit IgG (1:20,000 dilution; Abcam, Cambridge, UK; catalog number: ab6721). Unbound secondary antibodies were removed by washing thrice with wash buffer, followed by visualization of immunoreactive bands using ECL detection reagents. Films were scanned using the Azure c400 scanner (Azure Biosystems, San Francisco, CA, USA).

Transmission Electron Microscopy (TEM) Analysis

TEM observation was conducted following established protocols with minor modifications [33]. EV precipitates obtained by ultracentrifugation (10,000 ×g, 50,000 ×g, and 100,000 ×g) were mixed in a tube and fixed with 4% glutaraldehyde at 4 °C overnight. The fixed EVs pellet was encased in 4% agarose and fixed with a 2.5% glutaraldehyde fixative solution for 2 hours at 4 °C. Subsequently, the fixed agarose block was dehydrated, embedded, and sliced according to standard protocols. All transmission electron micrographs were captured using the JEM-1400 Plus transmission electron microscope (JEOL, Tokyo, Japan).

DNase Treatment

Prior to DNA extraction from EVs, the Turbo DNA-free Kit (Thermo Fisher Scientific, Waltham, MA, USA; catalog number: AM1907) was utilized to completely digest external DNA present on the surface of EVs. The optimal action condition of DNase I was achieved at 20 U/mL for 30 minutes. EVs sample (100 μL) were mixed with 2U of Turbo DNase in 10× Turbo DNase buffer then incubated at 37 °C for 30 minutes following the manufacturer's instructions. Subsequent steps were performed following the instructions for the kit. The Control group was treated with DNase I as follows: After adding Buffer AL (lysate), DNase I was applied, and the remaining steps were conducted with DNase I enzyme digestion.

DNA Extraction and Identification

DNA was isolated from samples using the QIAamp DNA Mini Kit (Qiagen, Hilden, Germany; Catalog number: 51306) following the manufacturer's instructions. Prior to DNA extraction, samples were treated with RNase A (10 mg/mL). Following DNA isolation, cellular DNA was eluted in 200 μL of Buffer AE, while EV DNA was eluted in 50 μL of Buffer AE. All DNA samples were stored at –20 °C. DNA concentrations were analyzed using the Infinite 200 PRO (TECAN, Männedorf, Switzerland) following the manufacturer's protocols. DNA size was analyzed using 4200 TapeStation Systems with High Sensitivity D5000 ScreenTape or genome DNA ScreenTape (Agilent Technologies, Santa Clara, CA, USA; catalog number: 5067-5584, 5067-5365) according to the manufacturer's instructions. DNA was resuspended in 1× DNA loading buffer and loaded onto a 1% agarose gel (Solarbio, Beijing, China; catalog number: A8201) and run at 100 V for 30 minutes. To identify the type of DNA, the agarose gel was stained with SYBR Green I (1:10,000 dilution in 1× TAE; Solarbio, Beijing, China; catalog number: S7567) for 30 minutes and observed under UV light.

Whole Genome Sequencing and Bioinformatic Analysis

DNA was sequenced on a Novaseq 6000 platform (Illumina, San Diego, CA, USA) with paired-end 150 bp reads. The raw sequencing data underwent quality filtering using fastp (v0.20.0, https://github.com/OpenGene/fastp). Subsequently, the reads were aligned to the reference mouse genome (mm10) using bwa (v0.7.8-r455, https://bio-bwa.sourceforge.net/). Raw single nucleotide polymorphism (SNP) and Insertion/Deletion (InDel) sets were called using SAMtools (v1.3.1, https://samtools.sourceforge.net/) with the following parameters: '-C 50-mpileup-m2-F 0.002-d 1000'. These sets were then filtered based on the following criteria: (1) Depth of the variant position >4; (2) Mapping quality >20. Copy number variations (CNVs) were detected using CNVnator (parameter: call 100) to identify potential deletions and duplications. Functional annotation of variants was performed using ANNOVAR (v2015Dec14, https://annovar.openbioinformatics.org/). Sequencing depth and read distribution were analyzed using SAMtools (v1.3.1, https://samtools.sourceforge.net/). Aligned read densities across the entire genome were calculated using 100 kb bins and visualized using Circos plots. A Venn diagram was generated using the online tool EVenn (http://www.ehbio.com/test/venn/) [34]. The DP4 data of the mutant loci were filtered from the variants data in VCF format, and the variant allele frequency (VAF) of the mutant loci was calculated by dividing the number of reads of the mutant loci in the DP4 data by the total number of reads at the loci. An evolutionary tree based on SNPs was constructed using Mega11 (https://www.megasoftware.net) [35]. The Neighbor-Joining algorithm was employed for tree construction, with the Bootstrap value set to 1000.

Journal of
BIOLOGICAL REGULATORS
and Homeostatic Agents

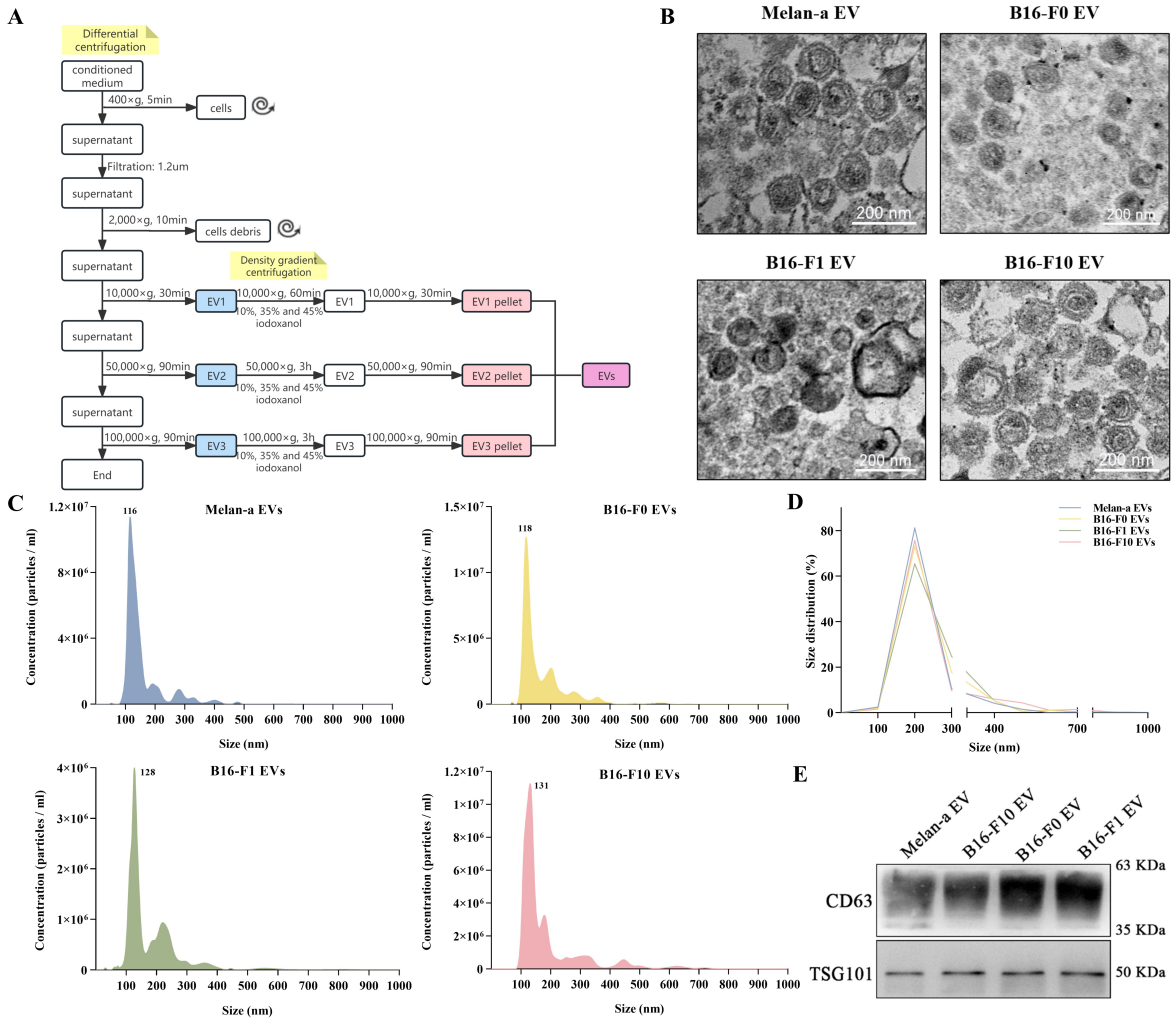

Fig. 1. Characterization of extracellular vesicles (EVs) isolated from melanocytes (Melan-a), B16-F0, B16-F1 and B16-F10 cells. (A) Schematic chart for EVs extraction process. (B) Transmission Electron Microscopy (TEM) images displaying the typical cup-shaped morphology of EVs. Scale bar: 200 nm. (C) Particle size distribution of isolated EVs. (D) Percentage distribution of EV sizes. (E) Western blot analysis showing the expression of EV-specific markers, Cluster of Differentiation 63 (CD63) and Tumor Susceptibility Gene 101 (TSG101), in isolated EVs.

Functional Enrichment Analysis

Gene Ontology (GO) enrichment analysis and Kyoto Encyclopedia of Genes and Genomes (KEGG) pathway enrichment analysis were conducted using Annotation, Visualization, and Integrated Discovery (DAVID; https://david.ncifcrf.gov/) [36]. The identified gene sets were categorized based on GO enrichment analysis and KEGG biochemical pathways. Molecular functions (MF), biological processes (BP), cellular components (CC), and pathways with a p-value ≤ 0.05 among the identified genes were explored for potential insights. Figures were generated using R (v4.0.2, https://www.r-project.org/) together with the ggplot2 package (https://github.com/tidyverse/ggplot2).

Protein-Protein Interactions (PPI) Analysis

Based on the gene variants, common trunk gene mutation and private gene mutations with different numbers and sites of mutations in B16-F0, B16-F1 and B16-F10 cell lines were collected. Trunk mutant genes were defined as those exhibiting distinct mutation sites or varying mutation counts among the common mutant genes. To prevent information loss, mutated genes shared between two samples were grouped into the cell line exhibiting lower metastatic potential. Subsequently, gene names were input into the STRING database (https://string-db.org/) for PPI analysis, generating interaction maps between proteins and exporting the data in tab-separated (tsv) format. The tsv-formatted data was then imported into Cytoscape (v3.9.0, Cytoscape Consortium, San Diego, CA, USA). The CytoNCA (https://apps.cytoscape.org/apps/cytonca) plug-in was employed

to calculate and analyze the Betweenness centrality of each node in the interaction network, and the results were visualized accordingly.

Results

Characterization of EVs Isolated from Melan-a, B16-F0, B16-F1, and B16-F10 Cells

EVs were isolated from cell culture supernatants through differential centrifugation and density gradient centrifugation (Fig. 1A). Morphological characteristics were visualized by TEM, size was measured by NTA, and protein characterization was performed by western blot (Fig. 1B–D). TEM data revealed that the EVs exhibited typical "cup-shaped" morphologies (Fig. 1B). NTA data showed that the size distribution of EVs secreted by the four cell lines ranged from 30 to 1000 nm, with the main peak (Mode) between 110–135 nm (Fig. 1C). Since the focus of this study is the EVs group containing exosomes, microvesicles, and apoptotic bodies of various sizes, we further analyzed the particle size distribution interval of the four groups of EVs at every 100 nm. The results indicated that approximately 90% of the total EVs in the four groups conformed to the size characteristics of exosomes (<300 nm), while approximately 10% were microvesicles and apoptotic bodies (400–700 nm) (Fig. 1D). Furthermore, EVs secreted by the four cell lines were positive for classical EV proteins, CD63, and TSG101, as determined by western blot (Fig. 1E). Collectively, these findings indicate that a mixture of EVs secreted by parent cells was successfully isolated from the cell culture supernatant.

Characterization of DNA in EVs Derived from Melan-a, B16-F0, B16-F1, and B16-F10 Cells

To determine the presence and localization of DNA within EVs, we isolated EVs from Melan-a, B16-F0, B16-F1, and B16-F10 cells and divided them into three samples for analysis. One sample remained untreated and therefore would contain DNA from the vesicle surface as well as internally protected DNA. Another sample underwent DNase I treatment to degrade DNA external to the EVs. The final sample was treated with DNase I following lysis of EVs, serving as a control. Post-DNase I treatment, DNA quantification was performed. Results indicated detectable DNA levels in the DNase I-treated sample. Conversely, no DNA was detectable in the lysed sample post-DNase I treatment, confirming that the EVs contained DNA and protected the internal DNA from digestion by DNase I (Fig. 2A). In addition, consistent with previous research [37,38], our data suggest that a significant portion of EV-associated DNA is external, which may relate to the mechanism of EV biogenesis or cargo repackaging.

Further comparative analysis of DNA contents from Melan-a and B16-F0/F1/F10 cell lines revealed that melanoma-derived EVs (B16-F0/F1/F10) contained more DNA, both externally and internally than EVs from normal Melan-a melanocytes (Fig. 2B). These observations suggest a potential correlation between the amount of DNA in EVs and the cell type or state.

Additionally, we employed SYBR Green I, a sensitive nucleic acid dye, to analyze the type of DNA associated with EVs. Under ultraviolet light, EV-associated DNA, before and after DNase I treatment, exhibited green fluorescence, similar to the fluorescence of double-stranded (dsDNA) markers and PCR products. In contrast, control single-stranded DNA (ssDNA) displayed orange fluorescence (Fig. 2C). These findings confirm the primary form of DNA in EVs is dsDNA.

The size distribution and structural characteristics of EV-associated DNA were assessed using chip-based capillary electrophoresis. Unlike the intact genomic DNA from parent cells, EV-associated DNA appeared as fragmented, ranging in size from 15 to 10,000 bp (Fig. 2D). Further comparative analysis of the distribution of DNA before and after DNase I treatment revealed that larger DNA fragments predominantly resided on the EV exterior, while smaller fragments were protected inside the EVs (Fig. 2D).

Collectively, our findings demonstrate that EVs from Melan-a, B16-F0, B16-F1, and B16-F10 cells contain stable dsDNA, characterized by a fragmented distribution ranging from 15 to 10,000 bp. Despite the predominance of external DNA, internal EV DNA exhibits greater stability, likely due to vesicular protection [27,39]. Those results prompt us to focus our subsequent experiments on the study of internal EV DNA.

Whole Genome Comparison of EVs and Parent Cells

To further determine whether EVs DNA mirrors the genomic information of their parent cells, we compared the EVs DNA and parental cell genomes. All samples underwent thorough sequencing quality assessment ensuring suitability for subsequent mutation detection and correlation analysis (**Supplementary Table 1**). Whole-genome sequencing results revealed comparable sequencing depth between EVs and cells across various loci, with EVs DNA covering the entire parental cell genome in an unbiased manner (Fig. 3A). To investigate the similarity between vesicles and the overall mutation spectrum of their parental cells, we further analyzed the number of mutation types present in vesicles and parental cells. Statistical analysis of detected mutation types indicated that the numbers of small fragment mutations (SNPs and InDels) in EVs were similar to those in parental cells. However, the quantity of detected CNVs in EVs and private mutations in EVs were significantly higher than in cells (Fig. 3B, **Supplementary Table 2**).

Moreover, we compared mutated genes detected in cells and their EVs. The majority of mutated genes were detected in EVs and parent cells, ranging from 69.5% to 77.1% (Fig. 3C). The proportion of mutated genes detected

Journal of
BIOLOGICAL REGULATORS
and Homeostatic Agents

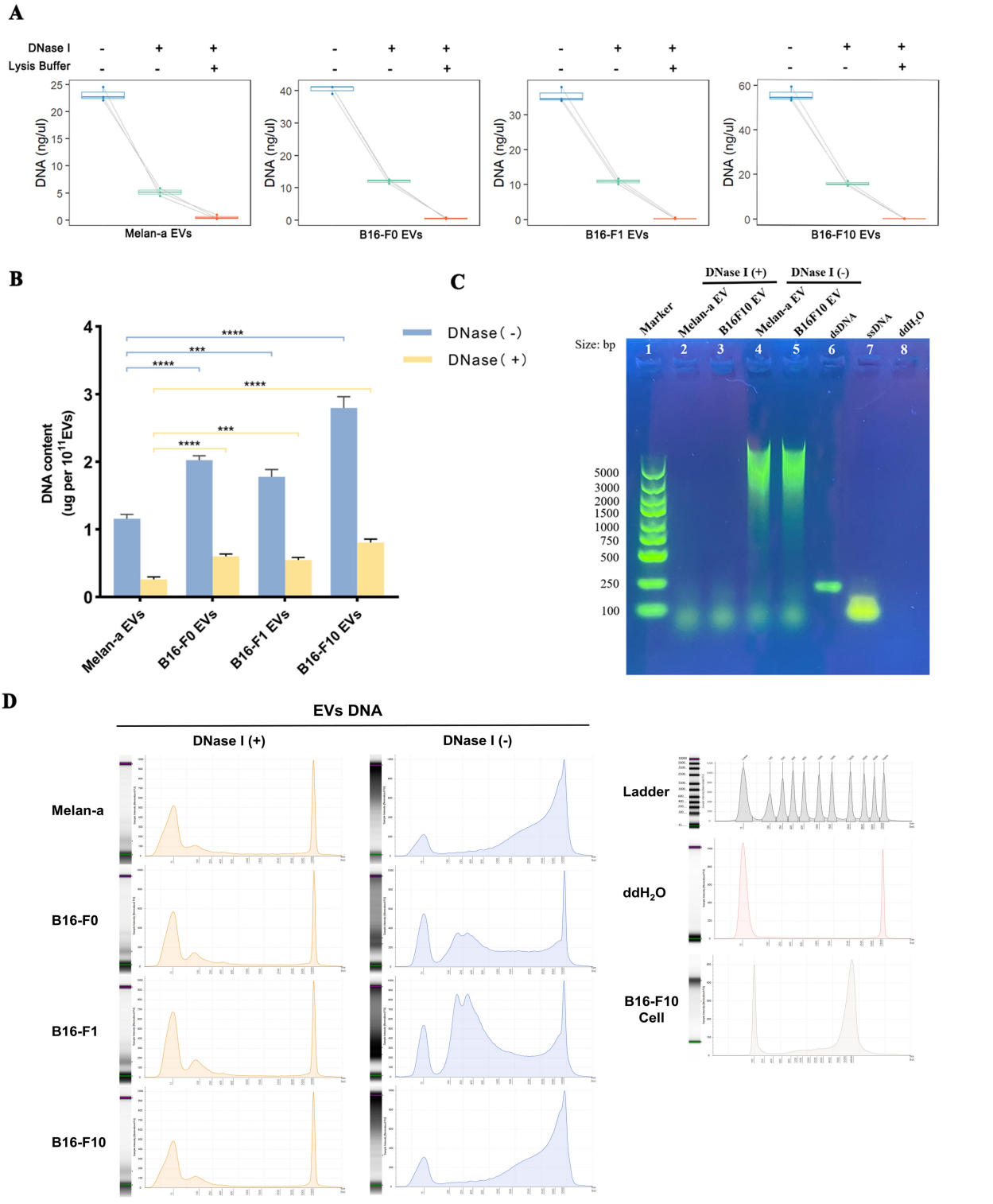

Fig. 2. Characterization of DNA in EVs isolated from Melan-a, B16-F0, B16-F1 and B16-F10 cells. (A) Quantification of DNA in EVs treated with DNase 1 before (Green) or after (Red) EV lysis, compared to untreated control (Blue). DNA content was measured in triplicates (n = 3). (B) Comparison of DNA amounts extracted from EVs of Melan-a, B16-F0, B16-F1, and B16-F10 cells (n = 3, ***$p < 0.001$, ****$p < 0.0001$). (C) Agarose gel electrophoresis of EV DNA stained with SYBR Green I. (D) Chip-based capillary electrophoresis of DNA by Aglient 4200 TapeStation system (v4.1.0.1488, Agilent Technologies, Santa Clara, CA, USA) using High Sensitivity D5000 ScreenTape (EVs DNA) or genome DNA ScreenTape (Cell DNA).

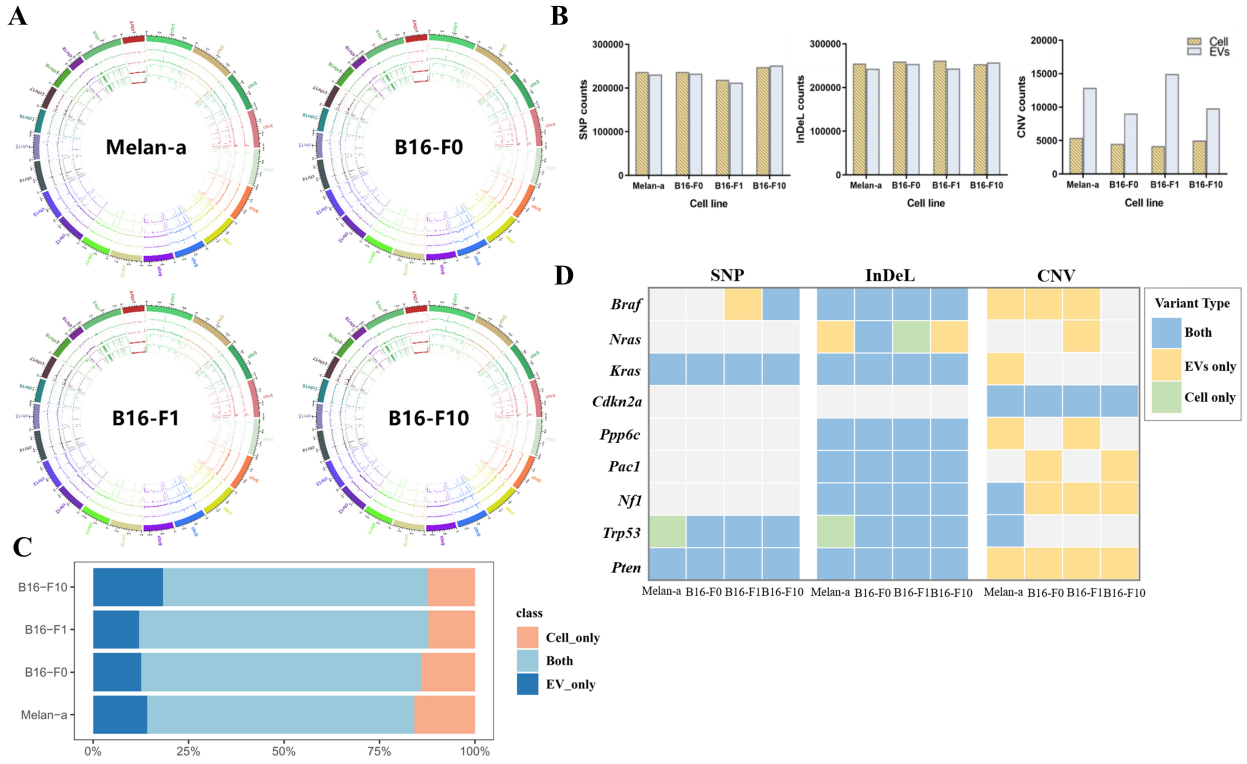

Fig. 3. Genome-wide analysis of EVs from Melan-a B16-F0, B16-F1 and B16-F10 cells. (A) Circular representation depicting the sequencing depth and coverage across each chromosome in whole-genome sequencing analysis of EV DNA compared to parental cell genome. The outermost circle represents cell sequencing depth, followed by EV sequencing depth, cell sequencing coverage, and EV sequencing coverage, respectively. (B) Comparison of single nucleotide polymorphism (SNP), Insertion/Deletion (InDel), and copy number variation (CNV) counts in EVs and parental cells. (C) Analysis of the number of mutant genes identified in EVs compared to parental cells. (D) Schematic representation illustrating the presence of melanoma-driven mutant genes in EVs and parental cells.

solely in cells ranged from 12.2% to 15.8%, while the proportion detected solely in EVs ranged from 12.1% to 18.2% (Fig. 3C). These findings suggest that EVs are reliable indicators of mutated genes present in parental cells. Driver genes, which play a crucial role in tumor development, were of particular interest. We selected nine melanoma driver genes (*Braf*, *Nras*, *Kras*, *Cdkn2a*, *Ppp6c*, *Rac1*, *Nf1*, *Trp53*, *Pten*) for comparative analysis based on public databases and existing literature [40]. The results demonstrated consistency rates ranging from 84.6%–100% in the detection of melanoma-related driver gene mutations between the four strains of EVs and cells.

Further analysis of mutation sites revealed high consistency in SNP mutation detection, with 85.8% (12/14) of mutations detected in cells and EVs. Additionally, mutations detected exclusively in cells or EVs accounted for 7.1% (1/14). For InDel mutations, the common detection rate between cells and EVs was 87.5% (28/32), while mutations detected exclusively in cells or EVs comprised 6.25% each (2/32). Moreover, in CNV mutations, the common detection rate between cells and EVs was 27.27% (6/22), with no mutations detected exclusively in cells (0/22) and a significantly higher proportion (54.5%; 16/22) detected exclusively in EVs (Fig. 3D). These findings underscore a robust consistency between EVs and cells in the detection of SNP and InDel mutation genes, while the consistency in the detection of CNV mutation genes is comparatively lower. Furthermore, despite the lower consistency in detecting CNV driver genes, all CNV mutations identified in cells were also observed in EVs (Fig. 3D). This observation suggests that in targeted testing of CNV mutations in specific genes, EVs may effectively represent the CNV mutation status of the parental cells.

Collectively, our findings indicate that EVs derived from Melan-a, B16-F0, B16-F1, and B16-F10 cell lines encapsulate the entire genomic content of their parental cells. The mutation information from the parental cells is also preserved in EVs, particularly SNP information. These findings suggest that EVs DNA has a good consistency with the genome of parent cells and can reflect the mutations of parent cells.

Evolutionary Relevant Mutation Profile in B16 Melanoma Cell Lines

Through Venn intersection analysis on missense mutation genes detected in three strains of melanoma cells, we

Journal of
BIOLOGICAL REGULATORS
and Homeostatic Agents

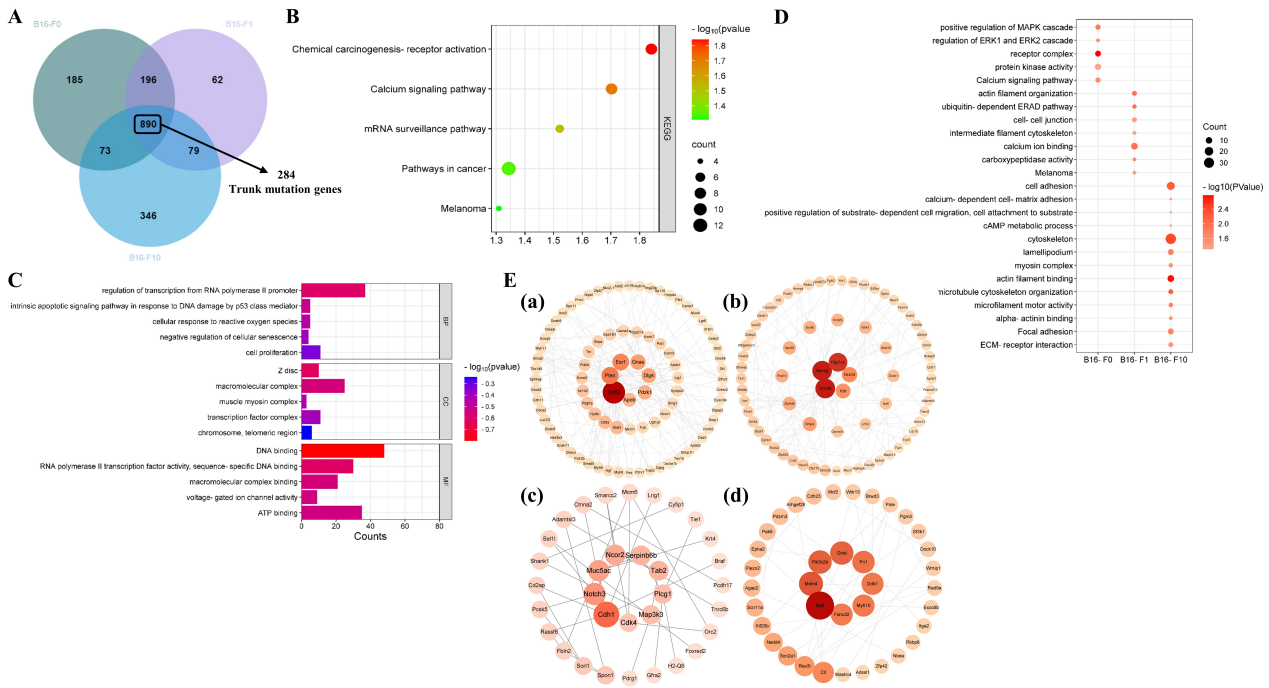

Fig. 4. Evolutionary relevant mutation profiles in B16 melanoma cell lines. (A) Venn diagram showing the overlap of missense mutation genes among the three B16 melanoma cell lines. (B,C) Enrichment analysis of trunk mutation genes in B16 melanoma cell lines, highlighting Kyoto Encyclopedia of Genes and Genomes (KEGG) pathway (B) and Gene Ontology (GO) terms (C). (D) Enrichment analysis of private mutation genes in B16 melanoma cell lines, focusing on GO terms and KEGG pathways. (E) PPI network depicting hub genes identified from the trunk and private mutation genes in B16 melanoma cell lines. Nodes with higher Betweenness values (>1000) are highlighted as hub genes. Subfigures (a–d) showcase trunk genes common across all B16 melanoma cell lines and private genes specific to B16-F0, B16-F1, and B16-F10 cells, respectively, highlighting variations in metastatic potential and biological processes.

identified common and private mutation genes in these cells with varying metastatic potentials (Fig. 4A). Considering that the individual genes may undergo mutations at distinct sites during the evolutionary trajectory of these cells, from the 890 common mutation genes, we selected genes with different or multiple mutation sites as the trunk mutation genes common to all three cell lines, resulting in a total of 284 genes (Fig. 4A). The trunk mutation genes were subjected to GO and KEGG functional annotation enrichment analysis using the DAVID online analysis platform. The analysis revealed the trunk mutation genes are mainly enriched in biological processes such as regulation of transcription from RNA polymerase II promoter, intrinsic apoptotic signaling pathway in response to DNA damage by *p53* class mediator, and cellular response to reactive oxygen species. Moreover, they were associated with cellular components such as Z disc, macromolecular complex, muscle myosin complex, as well as molecular functions including DNA binding and ATP binding (Fig. 4C). Pathway enrichment analysis demonstrated significant involvement of the trunk mutation genes in pathways such as chemical carcinogenesis-receptor activation, calcium signaling pathway, pathways in cancer, and melanoma (Fig. 4B).

Furthermore, we constructed a protein-protein interaction (PPI) network of the trunk mutation genes using the STRING database, which was further analyzed and visualized using Cytoscape (v3.9.0, Cytoscape Consortium, San Diego, CA, USA) software. Based on the Betweenness values, we identified hub genes with a centrality value >1000 (*Trp53*, *Pten*, *Esr1*, *Gnas*, *Dlg4*, *Pdzk1*, and *Apob*) and considered them as the trunk mutation genes characteristic of the B16 melanoma cell line (Fig. 4E).

Subsequently, we analyzed the private mutation genes of the three cell strains individually. Considering the possibility of shared mutations during the process of cell evolution and to avoid overlooking valuable information, we categorized mutation genes shared by two cell strains as the private mutation genes of the lower metastatic potential cell line for analysis. For example, the shared mutation genes in B16-F0 and B16-F1 cells were categorized as the private mutation genes of the B16-F0 cell. GO enrichment analysis and KEGG pathway analysis revealed distinct characteristics of the private mutation genes for each cell line.

The private mutation genes of B16-F0 cells primarily participated in biological processes such as positive regulation of the MAPK cascade and regulation of ERK1 and ERRK2 cascade. These genes were associated with cell

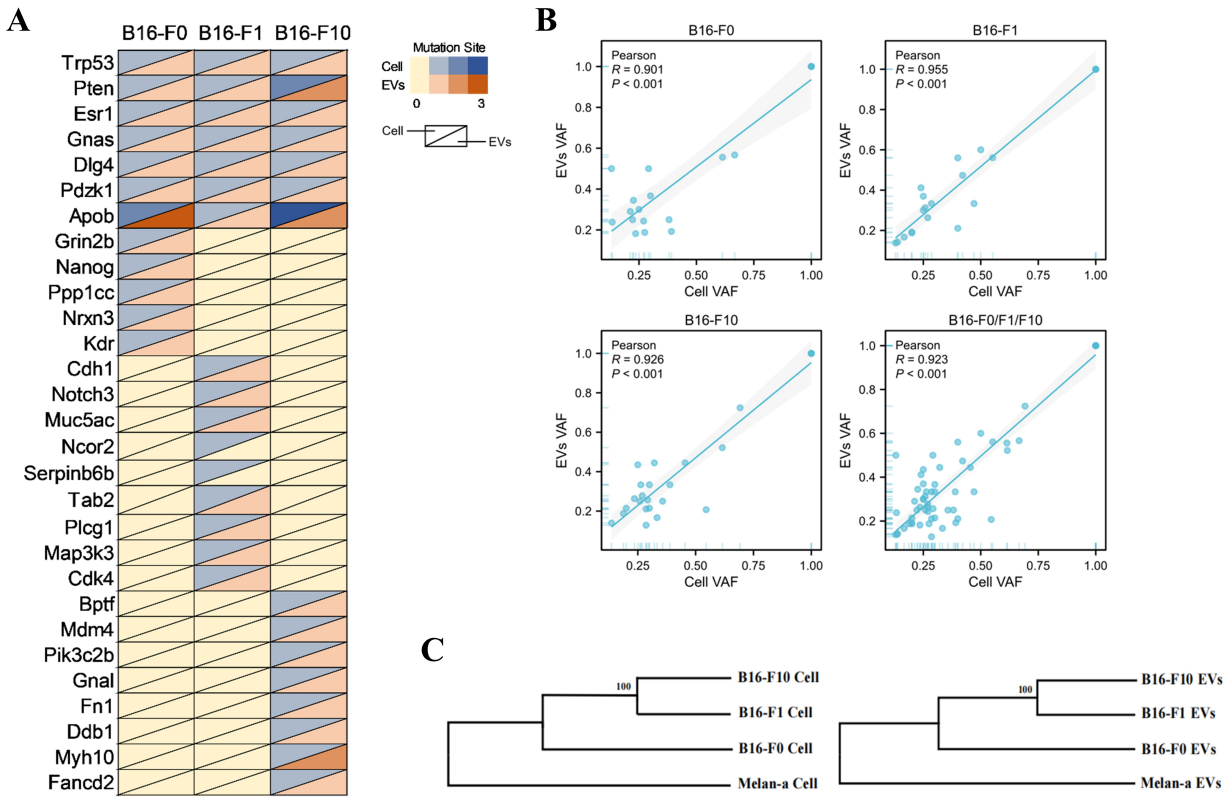

Fig. 5. Evolutionary relationship of parent cells reflected in EV DNA from longitudinal B16 melanoma cell lines. (A) Comparative analysis of the evolutionary relevant mutation profile between B16 melanoma cell lines and EVs. (B) Correlation between variant allele frequency (VAF) of evolutionary relevant mutation profiles identified in parental cell lines and EVs. (C) Construction of SNP-based evolutionary trees for three B16 melanoma cell lines and their corresponding EVs.

components like receptor complex and possessed molecular functions like protein kinase activity. Enriched pathways in KEGG included the calcium signaling pathway and circadian entrainment. The private mutation genes of B16-F1 cells were involved in biological processes such as actin filament organization and the ubiquitin-dependent ERAD pathway. These genes were associated with cell components such as cell-cell junction and the intermediate filament cytoskeleton, with molecular functions including calcium ion binding and carboxypeptidase activity (Fig. 4D). KEGG enrichment analysis showed significant involvement of the private mutation genes of B16-F1 cells in melanoma-related pathways.

Moreover, the private mutation genes of B16-F10 cells were primarily associated with biological processes such as cell adhesion (cell adhesion, calcium-dependent cell-matrix adhesion), cell migration (positive regulation of substrate-dependent cell migration, cell attachment to substrate), and cAMP metabolic processes. These genes were linked to cell components like cytoskeleton, lamellipodium, and myosin complex, with molecular functions including actin filament binding, microtubule cytoskeleton organization, and microfilament motor activity. KEGG analysis indicated enrichment in pathways related to Focal adhesion and ECM-receptor interaction (Fig. 4D). Our findings suggest that the private mutation genes in the three cell strains with varying metastatic potentials exhibit diverse functions, participating in distinct biological processes.

Using a similar methodology as screening the trunk mutation genes, we conducted individual PPI analyses on the three B16 melanoma cell lines, identifying the hub genes within the private mutation genes (Fig. 4E). Collectively, we compiled the trunk genes (*Trp53*, *Pten*, *Esr1*, *Gnas*, *Dlg4*, *Pdzk1*, *Apob*), along with the private mutation genes specific to each cell line: B16-F0 (*Grin2b*, *Nanog*, *Ppp1cc*, *Nrxn3*, *Kdr*), B16-F1 (*Cdh1*, *Notch3*, *Muc5ac*, *Ncor2*, *Serpinb6b*, *Tab2*, *Plcg1*, *Map3k3*, *Cdk4*), and B16-F10 (*Bptf*, *Mdm4*, *Pik3c2b*, *Gnal*, *Fn1*, *Ddb2*, *Myh10*, *Fancd2*), forming a mutation gene map related to the evolution of three different metastatic potential melanoma cells (**Supplementary Table 3**).

EVs DNA from Longitudinal B16 Melanoma Cell Lines Reflect the Evolutionary Relationship of Parent Cells

The mutations related to the evolutionary characteristics of melanoma cells with varying metastatic potentials,

Journal of
BIOLOGICAL REGULATORS
and Homeostatic Agents

as obtained from the preceding analysis, were compared to the corresponding EV samples to investigate their detection in EVs (Fig. 5A, **Supplementary Table 3**). The results revealed a detection rate of 95.3% (41/43) for genes associated with the evolutionary molecular features of the three cell lines in EVs. B16-F0 EVs encompassed the trunk mutation genes of the B16 melanoma cell line and the private mutation genes of B16-F0 cells, covering all mutation sites. Notably, an *Apob* gene mutation site was also detected in the EVs, which were not identified in the parental cells. Similarly, B16-F1 EVs harbored both the trunk mutation genes of the B16 melanoma cell line and the private mutation genes of B16-F1 cells, including *Cdh1*, *Notch3*, *Muc5ac*, *Tab2*, *Plcg1*, *Map3k3*, and *Cdk4,* with mutation sites consistent with those of the parent cells. However, the private mutation genes *Ncor2* and *Serpinb6b* were not identified in B16-F1 EVs. B16-F10 EVs contained all trunk mutation genes of the three cell lines and the private mutation genes of B16-F10 cells. However, only two *Apob* missense mutation sites were found, one fewer than in B16-F10 cells. Additionally, a missense mutation site in *Myh10* was detected exclusively in EVs. These findings suggest that EVs can effectively represent the evolutionary molecular features of parent cells.

Comparing the variant allele frequency (VAF) of melanoma cells with varying metastatic potentials and their corresponding EVs, the results demonstrated that the VAF levels in EVs were similar to those in cells and exhibited a strong positive correlation (Fig. 5B). These findings suggest that EVs may reflect changes in the mutation burden of parent cells.

To further explore whether EVs could also exhibit similar evolutionary relationships with their parental cells, we constructed evolutionary trees of the four cell strains and their corresponding EVs based on SNP data. The results indicated that the evolutionary relationships of B16-F0, B6-F1, and B16-F10 became farther away in sequence compared with those of Melan-a cells. The EVs secreted by the four cell lines exhibited consistent evolutionary relationships with their parental cells (Fig. 5C).

Discussion

Extracellular vesicles (EVs) are small lipid-bilayer membrane vesicles secreted by cells, encapsulating a variety of bioactive molecules such as DNA, RNA, proteins, and lipids, and regard as potential biomarkers [1,2,18]. While extracellular vesicle RNA and protein have been extensively studied, the characterization of extracellular vesicle-related DNA remains relatively unexplored. Our study presents several significant findings: (1) EVs derived from B16 melanoma cells contained stable dsDNA, which exhibits fragmentation in the range of 15 to 10,000 bp; (2) EVs DNA cover the entire genome of parent cells; (3) EVs DNA exhibits higher consistency with small fragment mutations (SNP, InDel) of parent cells, albeit with reduced consistency as mutational length increases; (4) EVs harbor mutant gene profiles associated with melanoma cell progression and exhibit comparable evolutionary relationships with parent cells. These findings significantly advance our understanding of the characteristics of EVs DNA. The presence of fragmented DNA within EVs, covering the entire genomic landscape and specific mutations of the parental cells, holds promising implications as a biomarker for disease diagnosis and treatment. The consistency of EV DNA with parental cell mutations, particularly those involved in melanoma progression, underscores the potential of EVs as a non-invasive tool for monitoring tumor evolution and identifying therapeutic targets.

Our study confirms the presence of stable dsDNA in EVs derived from Melan-a and B16 melanoma cell lines. The stability of DNA within EVs can be attributed to the protective effect of the complete lipid bilayer membrane. Additionally, we observed that EV DNA derived from melanoma cells exhibits fragmentation ranging from 15 to 10,000 bp, with long dsDNA fragments potentially contributing to DNA stability within EVs [41–43]. Notably, previous studies have reported the presence of single-stranded DNA (ssDNA) in EVs [19–21]. However, the reason of ssDNA was detected, such as variations in cell types or EV subpopulations, denaturation of dsDNA, or limitations of current techniques in accurately distinguishing short ss/ds DNA fragments, warrant further investigation [26,41]. The advancement of more precise assay methodologies will facilitate the exploration of the diverse types of EV DNA.

Furthermore, our findings from DNase I digestion assays revealed that a substantial portion (approximately 60%–70%) of melanoma EV-associated DNA is located on the surface of EVs rather than within the EVs. This observation aligns with previous reports, although differences in opinion about the proportion of DNA within EVs may be partly due to variations in cell origins and types [19]. The inclusion of all subpopulations of EVs in our study, including larger vesicles, may contribute to the higher proportion of DNA observed in melanoma EVs [26,41]. Therefore, investigating whole vesicles secreted by cells, rather than focusing on individual subpopulations, may provide valuable insights into the DNA content of EVs.

Moreover, we constructed PPI interaction networks for trunk mutant genes and specific mutant genes of the three cell lines, screening hub genes as evolutionary molecular characteristics of varying metastatic melanoma cells and integrating them into corresponding EVs. The results revealed a consistency rate of 95.3% (41/43) between EVs and parent cells, indicating that EVs from melanoma cells with varying metastatic potentials could accurately represent the molecular characteristics of parental cell evolution. Interestingly, we identified the *Apob* (exon29:c.T12491C) mutation in B16-F0 EVs, which was absent in B16-F0 cell.

Additionally, the *Myh10* (exon13:c.G1518A) mutation was detected in B16-F10 EVs despite its absence in the corresponding cells. Such differences in analysis may arise from errors and loss of mutation information due to inadequate sequencing depth and coverage [17]. Future studies should enhance sequencing depth and coverage to mitigate potential errors associated with sequencing technology.

The challenge of acquiring standardized clinical samples and their corresponding EVs constrained the scope of this study. To accurately explore the ability of EV DNA to monitor the dynamics of parental cell genomes, this study primarily relied on cell culture models and lacked the investigation of clinical samples. Building upon this groundwork, future endeavors should include sufficient clinical samples to further validate the efficacy of EV DNA in monitoring tumor dynamic changes.

Conclusions

This study elucidated that extracellular vesicles (EVs) derived from B16 melanoma cells contain stable double-stranded (dsDNA) that spans the entire parental cell genome. Despite challenges in mutation detection arising from current sequencing technology limitations, the findings underscore the capacity of EVs DNA effectively reflect the mutation profiles and dynamic alterations of melanoma cells with varying metastatic potentials. In summary, our study reveals the potential of EV DNA as a promising biomarker for dynamically monitoring tumor evolution, and providing a theoretical foundation for monitoring tumor progression by using EVs DNA.

Availability of Data and Materials

The datasets used or analyzed during the present study are available from the corresponding author on reasonable request.

Author Contributions

LQF, JB and XLC conceived the research, analyzed the data, wrote the manuscript and designed the experiments. XLC, YQH, LXW and YZJ performed the experiments. All authors were involved in editing the manuscript. All authors have read and agreed to the published version of the manuscript. All authors have participated sufficiently in the work to take public responsibility for appropriate portions of the content and agreed to be accountable for all aspects of the work in ensuring that questions related to its accuracy or integrity.

Ethics Approval and Consent to Participate

Not applicable.

Acknowledgment

Not applicable.

Funding

This research received no external funding.

Conflict of Interest

The authors declare no conflict of interest.

Supplementary Material

Supplementary material associated with this article can be found, in the online version, at https://doi.org/10.23812/j.biol.regul.homeost.agents.20243806.423.

References

[1] Théry C, Ostrowski M, Segura E. Membrane vesicles as conveyors of immune responses. Nature Reviews. Immunology. 2009; 9: 581–593.

[2] van Niel G, D'Angelo G, Raposo G. Shedding light on the cell biology of extracellular vesicles. Nature Reviews. Molecular Cell Biology. 2018; 19: 213–228.

[3] Théry C, Witwer KW, Aikawa E, Alcaraz MJ, Anderson JD, Andriantsitohaina R, *et al*. Minimal information for studies of extracellular vesicles 2018 (MISEV2018): a position statement of the International Society for Extracellular Vesicles and update of the MISEV2014 guidelines. Journal of Extracellular Vesicles. 2018; 7: 1535750.

[4] Lässer C, Jang SC, Lötvall J. Subpopulations of extracellular vesicles and their therapeutic potential. Molecular Aspects of Medicine. 2018; 60: 1–14.

[5] Willms E, Cabañas C, Mäger I, Wood MJA, Vader P. Extracellular Vesicle Heterogeneity: Subpopulations, Isolation Techniques, and Diverse Functions in Cancer Progression. Frontiers in Immunology. 2018; 9: 738.

[6] Skotland T, Sandvig K, Llorente A. Lipids in exosomes: Current knowledge and the way forward. Progress in Lipid Research. 2017; 66: 30–41.

[7] Skotland T, Sagini K, Sandvig K, Llorente A. An emerging focus on lipids in extracellular vesicles. Advanced Drug Delivery Reviews. 2020; 159: 308–321.

[8] Ghadami S, Dellinger K. The lipid composition of extracellular vesicles: applications in diagnostics and therapeutic delivery. Frontiers in Molecular Biosciences. 2023; 10: 1198044.

[9] Kim KM, Abdelmohsen K, Mustapic M, Kapogiannis D, Gorospe M. RNA in extracellular vesicles. Wiley Interdisciplinary Reviews. RNA. 2017; e1413.

[10] Garcia-Martin R, Wang G, Brandão BB, Zanotto TM, Shah S, Kumar Patel S, *et al*. MicroRNA sequence codes for small extracellular vesicle release and cellular retention. Nature. 2022; 601: 446–451.

[11] Kirian RD, Steinman D, Jewell CM, Zierden HC. Extracellular vesicles as carriers of mRNA: Opportunities and challenges in diagnosis and treatment. Theranostics. 2024; 14: 2265–2289.

[12] Macedo-da-Silva J, Santiago VF, Rosa-Fernandes L, Marinho CRF, Palmisano G. Protein glycosylation in extracellular vesicles: Structural characterization and biological functions. Molecular Immunology. 2021; 135: 226–246.

[13] Hánělová K, Raudenská M, Masařík M, Balvan J. Protein cargo

Journal of
BIOLOGICAL REGULATORS
and Homeostatic Agents

in extracellular vesicles as the key mediator in the progression of cancer. Cell Communication and Signaling. 2024; 22: 25.

[14] Li D, Lai W, Fan D, Fang Q. Protein biomarkers in breast cancer-derived extracellular vesicles for use in liquid biopsies. American Journal of Physiology. Cell Physiology. 2021; 321: C779–C797.

[15] Cai J, Guan W, Tan X, Chen C, Li L, Wang N, *et al*. SRY gene transferred by extracellular vesicles accelerates atherosclerosis by promotion of leucocyte adherence to endothelial cells. Clinical Science. 2015; 129: 259–269.

[16] Zomer A, Maynard C, Verweij FJ, Kamermans A, Schäfer R, Beerling E, *et al*. In Vivo imaging reveals extracellular vesicle-mediated phenocopying of metastatic behavior. Cell. 2015; 161: 1046–1057.

[17] Pietrowska M, Zebrowska A, Gawin M, Marczak L, Sharma P, Mondal S, *et al*. Proteomic profile of melanoma cell-derived small extracellular vesicles in patients' plasma: a potential correlate of melanoma progression. Journal of Extracellular Vesicles. 2021; 10: e12063.

[18] Ferguson S, Yang KS, Weissleder R. Single extracellular vesicle analysis for early cancer detection. Trends in Molecular Medicine. 2022; 28: 681–692.

[19] Thakur BK, Zhang H, Becker A, Matei I, Huang Y, Costa-Silva B, *et al*. Double-stranded DNA in exosomes: a novel biomarker in cancer detection. Cell Research. 2014; 24: 766–769.

[20] Kahlert C, Melo SA, Protopopov A, Tang J, Seth S, Koch M, *et al*. Identification of double-stranded genomic DNA spanning all chromosomes with mutated KRAS and p53 DNA in the serum exosomes of patients with pancreatic cancer. The Journal of Biological Chemistry. 2014; 289: 3869–3875.

[21] Lee TH, Chennakrishnaiah S, Audemard E, Montermini L, Meehan B, Rak J. Oncogenic ras-driven cancer cell vesiculation leads to emission of double-stranded DNA capable of interacting with target cells. Biochemical and Biophysical Research Communications. 2014; 451: 295–301.

[22] Ghanam J, Chetty VK, Barthel L, Reinhardt D, Hoyer PF, Thakur BK. DNA in extracellular vesicles: from evolution to its current application in health and disease. Cell & Bioscience. 2022; 12: 37.

[23] Fischer S, Cornils K, Speiseder T, Badbaran A, Reimer R, Indenbirken D, *et al*. Indication of Horizontal DNA Gene Transfer by Extracellular Vesicles. PLoS ONE. 2016; 11: e0163665.

[24] Wang L, Li Y, Guan X, Zhao J, Shen L, Liu J. Exosomal double-stranded DNA as a biomarker for the diagnosis and preoperative assessment of pheochromocytoma and paraganglioma. Molecular Cancer. 2018; 17: 128.

[25] Balaj L, Lessard R, Dai L, Cho YJ, Pomeroy SL, Breakefield XO, *et al*. Tumour microvesicles contain retrotransposon elements and amplified oncogene sequences. Nature Communications. 2011; 2: 180.

[26] Lázaro-Ibáñez E, Sanz-Garcia A, Visakorpi T, Escobedo-Lucea C, Siljander P, Ayuso-Sacido A, *et al*. Different gDNA content in the subpopulations of prostate cancer extracellular vesicles: apoptotic bodies, microvesicles, and exosomes. The Prostate. 2014; 74: 1379–1390.

[27] Jin Y, Chen K, Wang Z, Wang Y, Liu J, Lin L, *et al*. DNA in serum extracellular vesicles is stable under different storage conditions. BMC Cancer. 2016; 16: 753.

[28] Malkin EZ, Bratman SV. Bioactive DNA from extracellular vesicles and particles. Cell Death & Disease. 2020; 11: 584.

[29] Carvalho J, Oliveira C. Extracellular Vesicles - Powerful Markers of Cancer EVolution. Frontiers in Immunology. 2015; 5: 685.

[30] Poste G, Doll J, Hart IR, Fidler IJ. In vitro selection of murine B16 melanoma variants with enhanced tissue-invasive properties. Cancer Research. 1980; 40: 1636–1644.

[31] Kim YS, Shin S, Yin JH, Park J, Jung SH, Chung YJ. Single-cell RNA sequencing reveals the existence of pro-metastatic subpopulation within a parental B16 murine melanoma cell line. Biochemical and Biophysical Research Communications. 2022; 613: 120–126.

[32] Fidler IJ. Biological behavior of malignant melanoma cells correlated to their survival in vivo. Cancer Research. 1975; 35: 218–224.

[33] Wang C, Wang Y, Chang X, Ba X, Hu N, Liu Q, *et al*. Melanoma-Derived Exosomes Endow Fibroblasts with an Invasive Potential via miR-21 Target Signaling Pathway. Cancer Management and Research. 2020; 12: 12965–12974.

[34] Chen T, Zhang H, Liu Y, Liu YX, Huang L. EVenn: Easy to create repeatable and editable Venn diagrams and Venn networks online. Journal of Genetics and Genomics. 2021; 48: 863–866.

[35] Tamura K, Stecher G, Kumar S. MEGA11: Molecular Evolutionary Genetics Analysis Version 11. Molecular Biology and Evolution. 2021; 38: 3022–3027.

[36] Huang DW, Sherman BT, Lempicki RA. Systematic and integrative analysis of large gene lists using DAVID bioinformatics resources. Nature Protocols. 2009; 4: 44–57.

[37] Liu H, Tian Y, Xue C, Niu Q, Chen C, Yan X. Analysis of extracellular vesicle DNA at the single-vesicle level by nano-flow cytometry. Journal of Extracellular Vesicles. 2022; 11: e12206.

[38] Lázaro-Ibáñez E, Lässer C, Shelke GV, Crescitelli R, Jang SC, Cvjetkovic A, *et al*. DNA analysis of low- and high-density fractions defines heterogeneous subpopulations of small extracellular vesicles based on their DNA cargo and topology. Journal of Extracellular Vesicles. 2019; 8: 1656993.

[39] García-Silva S, Gallardo M, Peinado H. DNA-Loaded Extracellular Vesicles in Liquid Biopsy: Tiny Players With Big Potential? Frontiers in Cell and Developmental Biology. 2021; 8: 622579.

[40] Bailey MH, Tokheim C, Porta-Pardo E, Sengupta S, Bertrand D, Weerasinghe A, *et al*. Comprehensive Characterization of Cancer Driver Genes and Mutations. Cell. 2018; 174: 1034–1035.

[41] Vagner T, Spinelli C, Minciacchi VR, Balaj L, Zandian M, Conley A, *et al*. Large extracellular vesicles carry most of the tumour DNA circulating in prostate cancer patient plasma. Journal of Extracellular Vesicles. 2018; 7: 1505403.

[42] Takahashi A, Okada R, Nagao K, Kawamata Y, Hanyu A, Yoshimoto S, *et al*. Exosomes maintain cellular homeostasis by excreting harmful DNA from cells. Nature Communications. 2017; 8: 15287.

[43] Cutter AR, Hayes JJ. A brief review of nucleosome structure. FEBS Letters. 2015; 589: 2914–2922.